Numerical modeling of the optical properties of hydrogenated amorphous siliconbased pin solar cells deposited on rough transparent conducting oxide substrates

F. Leblanc, J. Perrin, and J. Schmitt

Citation: J. Appl. Phys. **75**, 1074 (1994); doi: 10.1063/1.356489
View online: http://dx.doi.org/10.1063/1.356489
View Table of Contents: http://jap.aip.org/resource/1/JAPIAU/v75/i2
Published by the American Institute of Physics.

Numerical modeling of the optical properties of hydrogenated amorphous-silicon-based *p-i-n* solar cells deposited on rough transparent conducting oxide substrates

F. Leblanc[a] and J. Perrin
Laboratoire de Physique des Interfaces et des Couches Minces, CNRS UPR AO 258, Ecole Polytechnique, 91128 Palaiseau Cedex, France

J. Schmitt[b]
Solems S.A., 3 rue Léon Blum, Z.I. Les Glaises, 91124 Palaiseau Cedex, France

(Received 19 April 1993; accepted for publication 4 October 1994)

Hydrogenated amorphous-silicon (*a*-Si:H) -based solar cells consist of two electrodes and a *p-i-n* structure, deposited on glass substrates. Depositing the *p-i-n* layers and the back metallic electrode on an optically rough transparent conducting oxide (TCO) electrode enhances the absorption of the incident light in the active *i* layer: Light is scattered at the rough front interface and is partially trapped in the high refraction index layer, as in a waveguide. In addition TCO roughness increases the front transmission coefficient, increasing the amount of light in the active layer. TCO texture yields a relative increase of the conversion efficiency up to 30%. A semiempirical model of thin-film solar-cell optics is presented, taking into account the interface roughness by introducing experimentally derived scattering coefficients and treating the propagation of specular light in a rigorous way. Numerically simulated spectral response and total reflectance of standard solar cells deposited on different TCO textures are compared to experimental data. The results show a better fit to measured characteristics than simulations obtained by previous semiempirical modeling. Improvements mainly come from the light propagation calculation. According to the model, the number of passes incident light may make through the active *i* layer reaches six for the most efficient cell. As an example of the model's main application, the enhancement of the conversion efficiency that would be expected from an optimized TCO layer is calculated for each texture studied and for different back metallizations.

I. INTRODUCTION

The main interest in *a*-Si:H solar cells comes from thin-film deposition technology. This technology allows low material costs and devices to be deposited over large areas. We present in Fig. 1 a schematic description of a typical *a*-Si:H-based *p-i-n* solar cell. In order to enhance the conversion efficiency of the cells, both electronic and optical properties have to be investigated. The aim is to maximize incident light absorption in the active layer and to collect all the photogenerated carriers. In the past few years, improvement of the optical properties has been a dominating factor in device conversion enhancement. As a matter of fact, transparent conducting oxide (TCO) texture is a key issue: It reduces optical reflection loss at the TCO/silicon interface and greatly increases light diffusion. Weakly absorbed radiation, when scattered, can be partly trapped in the high refraction index layer because of total internal reflection at the interfaces. Due to the high refraction index of *a*-Si:H ($n \approx 3.7$), optical confinement occurs in the active layer, allowing light to experience several passes through this layer. When deposited on appropriately rough TCO substrates, large area conversion efficiencies integrated over the conventional AM1.5 solar spectrum reach 8.5% for a *p-i-n/p-i-n* tandem structure, as reported by Yoshida *et al.*;[1] so far device optical optimization was based on empirical approaches.

The TCO texture consists of microcrystallites whose size is comparable to visible light wavelengths. Because of the broad distribution of grain size and shape, the interaction between incident light and the multilayer structure is complex. A rigourous three-dimensional electromagnetic treatment would require enormous computation facilities, so a semiempirical approach is usually chosen. Different groups, namely Deckman *et al.*,[2] Shade and Smith,[3] and Morris *et al.*,[4] have already addressed this problem by more or less sophisticated semiempirical modeling.

An original semiempirical model is presented here. Diffuse reflectances R_d and transmittances T_d due to interface roughness are derived from angular-resolved photometric measurements, and are used as input parameters to the numerical program. In our model, the electromagnetic field's specular reflection and transmission coefficients are assumed to be proportionnal to the classical Fresnel coefficients, the proportionality factor depending on the amount of total diffused light. Consequently specular light coherence is kept and specular interferential effects, which may be observed experimentally with a moderately rough TCO substrate, are taken into account. With the support of experimental results and as a simplifying assumption, phase coherence between diffused light and incident light is assumed to be lost at the interface. Thus, at a given rough

[a]Also with: SOLEMS S.A., 3 rue Leon Blum, Z.I. Les Glaises, 91124 Palaiseau Cedex, France.
[b]Present address: Balzers Display Technology S.A., 5 rue Léon Blum, Z.I. Les Glaises, 91124 Palaiscau Cedex, France.

 0021-8979/94/75(2)/1074/14/$6.00

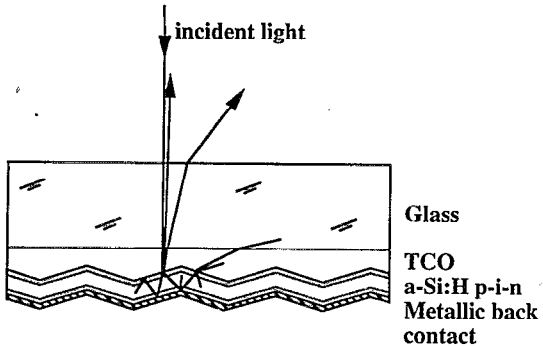

FIG. 1. Schematic description of *a*-Si:H-based *p-i-n* solar cells deposited on rough TCO substrates.

interface, diffused light is similar to a new source emitting inside the stack. After sampling the space in several directions, the light propagating along each of these directions is assumed to be a plane wave. This diffuse light is once again partly diffused and partly specularly transmitted or reflected at the rough interfaces. Each of the components coming from this second diffusion is then treated as in the first step. At each step, electromagnetic-field amplitudes at each side of every interface are calculated, allowing the derivation of the Poynting vector flux and, thus, the amount of absorbed light in each layer. In this way, multiple diffusion is taken into account. Instead of adding the absorbed flux at each successive step, we have developed a matrix method procedure, based on the formal similarity between the calculation process for the *n*-times-diffused light and the once-diffused light propagation. This approach is also applicable to CdTe or $CuInSe_2$ thin-film solar cells.

First of all, the consistency and reliability of the numerical code are verified by calculating the thermodynamic light trapping limit analyzed by Yablonovitch[5] and Yablonovitch and Cody.[6] Angular-resolved-reflectance (ARR) and transmittance (ART) measurements are then presented at four wavelengths covering the visible spectrum for bare TCO films, metallized TCO, and *a*-Si:H-covered TCO films. Absorptances of standard solar cells (absorptance in a given layer being defined as the fraction of incident photons that are absorbed in the layer) are calculated, using the derived diffuse reflectance and transmittance at the rough interfaces. Calculated cell total reflectance and calculated absorptance in the *i* layer are compared to measured total reflectance $R(\lambda)$ and quantum spectral response $Q(\lambda)$ under negative bias of the solar cell. Under negative bias, the *a*-Si:H collection efficiency of photogenerated carriers is close to one, and therefore the absorptance in the *i* layer and $Q(\lambda)$ are equal. Comparison between the present numerical modeling and another analytical model is discussed.

II. STATE OF THE ART

A. Classical thin-film theory

The propagation of an electromagnetic plane wave incident upon a stack of thin layers separated by ideally flat interfaces can be easily solved from the classical Maxwell equations. For non-normal incidence, the incident light is divided into two polarization modes, the transverse electric (TE) and transverse magnetic (TM) modes, transverse meaning perpendicular to the plan of incidence. It is common practice to associate the transverse electric field $\mathbf{E}_s$ with the TE mode, and the parallel electric field $\mathbf{E}_p$ with the TM mode. In absorbing media, $\mathbf{E}_p$ is no longer linearly polarized (the end point of $\mathbf{E}_p$ traces an ellipse in the plan of incidence).[7] Thus, in this case, the direction of $\mathbf{E}_p$ is not constant, and the scalar expression of the Poynting vector $\mathbf{\Sigma}$ [see Eq. (6)] becomes complicated. For the TM mode, it is convenient to choose the transverse magnetic field $\mathbf{H}_s$, since $\mathbf{H}_s$ remains transverse as it propagates through the stack (as does $\mathbf{E}_s$ for the TE mode). For the TE (TM) polarization mode, the field's amplitude reflection and transmission coefficients $r_{\mathrm{TE}_{12}}$ and $t_{\mathrm{TE}_{12}}$ ($r_{\mathrm{TM}_{12}}$ and $t_{\mathrm{TM}_{12}}$) at the interface between two layers 1 and 2 depend on the electromagnetic wave angle of incidence. It is convenient to introduce the wave vector $\mathbf{k}$ and to choose as the angular variable k_{xy}, the component of $\mathbf{k}$ lying in the interface plane xy. According to Descartes–Snell's law, k_{xy} remains constant at the reflection and refraction at each interface, and therefore is an invariant variable when specular light propagates through the entire stack. Thus, $r_{\mathrm{TE}_{12}}$, $t_{\mathrm{TE}_{12}}$, $r_{\mathrm{TM}_{12}}$, and $t_{\mathrm{TM}_{12}}$ are given as functions of k_{xy} by

$$r_{\mathrm{TE}_{12}}=\frac{k_{1_z}-k_{2_z}}{k_{1_z}+k_{2_z}},\quad t_{\mathrm{TE}_{12}}=\frac{2k_{1_z}}{k_{1_z}+k_{2_z}},$$
$$r_{\mathrm{TM}_{12}}=\frac{\frac{k_{1_z}}{\epsilon_1}-\frac{k_{2_z}}{\epsilon_2}}{\frac{k_{1_z}}{\epsilon_1}+\frac{k_{2_z}}{\epsilon_2}},\quad t_{\mathrm{TM}_{12}}=\frac{2\frac{k_{1_z}}{\epsilon_1}}{\frac{k_{1_z}}{\epsilon_1}+\frac{k_{2_z}}{\epsilon_2}}, \tag{1}$$

where

$$k_{m_z}=\left[\left(\frac{2\pi}{\lambda}\right)^2\epsilon_m-k_{xy}^2\right]^{1/2}\quad (m=1,2), \tag{2}$$

due to

$$\mathbf{k_m}\cdot\mathbf{k_m}=\left(\frac{2\pi}{\lambda}\right)^2\tilde{n_m}^2=\left(\frac{2\pi}{\lambda}\right)^2\epsilon_m, \tag{3}$$

where $\tilde{n_m}$ and ϵ_m are the complex refractive index and dielectric permittivity of the m medium, and λ the wavelength in vacuum.

The total electromagnetic field at each interface of the entire stack is the sum of the components coming from multiple reflection and refraction. Instead of calculating and successively adding each of these components, the total electromagnetic field is directly derived by using the powerful matrix method of Abeles.[7,8] At a given interface between two media m and $m+1$, in the case of the TE mode (for the TM mode, the magnetic-field amplitude H replaces the electric field amplitude E), fields propagating in both directions $E_{m,+}$ and $E_{m,-}$ in the medium m, are correlated to the fields $E_{m+1,+}$ and $E_{m+1,-}$ propagating in the medium $m+1$ by the interface matrix $I_{m/m+1}$ given by

$$I_{m/m+1}=\frac{1}{t_{\mathrm{TE}_{m,m+1}}}\begin{pmatrix}1 & r_{\mathrm{TE}_{m,m+1}}\\ r_{\mathrm{TE}_{m,m+1}} & 1\end{pmatrix}. \quad (4)$$

Field propagation through layer m is described by a diagonal propagation matrix P_m,

$$P_m=\begin{pmatrix}\exp(-ik_z l_m) & 0\\ 0 & \exp(+ik_z l_m)\end{pmatrix}, \quad (5)$$

where l_m is the layer thickness and $i^2=-1$. The total field is related to the field in the surrounding media by multiplying the $I_{m/m+1}$ and P_m matrices. In the case of an N-layer stack surrounded by two semi-infinite media 0 and $N+1$, the boundary conditions ($E_{N+1,-}=0$ and $E_{\mathrm{incident}}=E_{0,+}$) allow the calculation of the field in each layer, as a function of E_{incident}.

The Poynting vector $\boldsymbol{\Sigma}$ correlates the total electromagnetic field with the electromagnetic energy transport through the stack. Its flux through a unit area of interface surface unit is the power flux passing through this surface. $\boldsymbol{\Sigma}$ is given by

$$\boldsymbol{\Sigma}=\tfrac{1}{2}\,\mathrm{Re}(\mathbf{E}\times\mathbf{H}^*), \quad (6)$$

where Re (Im) refers to the real (imaginary) part of a complex vector, and * to the conjugation operator. When the total electromagnetic field is known, the flux Σ_z of $\boldsymbol{\Sigma}$ through any xy section can easily be calculated. For the TE mode,

$$\Sigma_z=\frac{1}{2\omega\mu}\left[\mathrm{Re}(k_z)(|E_+|^2-|E_-|^2)\right.$$
$$\left.+2\,\mathrm{Im}(k_z)\mathrm{Im}(E_+^* E_-)\right], \quad (7)$$

where the permeability μ equals the permeability of vacuum μ_0, for nonmagnetic media. For the TM mode

$$\Sigma_z=\frac{1}{2\omega}\left[\mathrm{Re}\left(\frac{k_z}{\epsilon}\right)(|H_+|^2-|H_-|^2)\right.$$
$$\left.+2\,\mathrm{Im}\left(\frac{k_z}{\epsilon}\right)\mathrm{Im}(H_+^* H_-)\right]. \quad (8)$$

The absorptance in each layer A_m is obtained by taking the difference of the power flux through the top interface and the bottom interface of the layer,

$$A_m=\frac{\Sigma_{z m\mathrm{top}}-\Sigma_{z m\mathrm{bottom}}}{\Sigma_z^{\mathrm{inc}}}. \quad (9)$$

This classical thin-film method takes into account light coherence and applies to flat interfaces. When using this method for a-Si:H p-i-n solar cells, interference peaks are predicted in the i layer absorptance and in the $R(\lambda)$ curves. Experimentally the i-layer absorptance is obtained by measuring $Q(\lambda)$, and $R(\lambda)$ is derived by measuring the sum of the specular and diffuse components of the reflectance. Although the predicted interference peaks are clearly observed in the experimental $Q(\lambda)$ and $R(\lambda)$ curves when the p-i-n layers are deposited on smooth or moderately rough TCO, they completely disappear on highly textured TCO. Moreover, the $Q(\lambda)$ curve integrated over the AM1.5 solar spectrum usually underestimates the measured conversion efficiency of a solar cell deposited on textured TCO whereas it gives an upper limit of the conversion efficiency of a solar cell deposited on smooth TCO. These findings reveal that the interface roughness has to be taken into account for a correct modeling of the optical absorptances and power balance in a solar cell.

TCO texture features reach a few tenths of microns which is comparable to visible wavelengths. Therefore, the classical dipole perturbative theory,[9] based on the introduction of current densities at the rough interface and on the assumption that the mean spatial frequencies are higher than the incident radiation frequency, is not useful. One must directly solve the Maxwell equations by taking into account the exact surface topology and derive the electromagnetic field in the entire space. "Exact" methods have been developed by Maystre,[10] by Saillard and Maystre,[11] and by DeSanto.[12] Their extension to three-dimensional randomized surfaces is still in progress. Moreover, they require the most powerful calculation tools, which is obviously an obstacle for a routine application in an industrial research and development laboratory.

B. Mie scattering theory

The scattering properties of small conducting particles embedded in a dielectric medium have been analytically derived from the Maxwell equations by Mie. Mie scattering theory has already been introduced to analyze TCO surface scattering properties.[13,14] The key factors are the ratio of particle size to wavelength and the relative index of refraction of the particles. The correlation between Mie theory and experimental diffuse transmittance of bare TCO films has been reported by O'Dowd.[13] In order to model the optical properties of solar cells, Shade and Smith[14] compared the diffuse reflectance and transmittance of TCO/air and TCO/metal interfaces by using Mie theory, but the model they have proposed still belongs to the semi-empirical model class (see below). This theory is difficult to apply in the case of a-Si:H solar cells because the grain size distribution has to be taken into account and because multiple scattering may occur in the stack. As far as we know, a complete modeling based on Mie scattering theory still has to be proposed.

C. Light-trapping limit from statistical ray optics

The maximum increase of the absorptance in the i layer due to TCO roughness has been studied by Yablonovitch and Cody.[6] Consider a layer with an index of refraction $\tilde{n}=n+i\kappa$, covered at the back interface by an ideal reflector (see Fig. 2), and such that complete randomization occurs in the layer (i.e., light is totally uniformly distributed in the layer or, in other words, the luminance is constant). The mean transmittance coefficient from the air to the layer is written as T_{inc} and the mean transmittance coefficient from the layer to the air as T_{esc}. According to statistical ray optics, when the layer absorption coefficient α tends to zero ($\alpha=4\pi\kappa/\lambda$), the absorptance enhancement

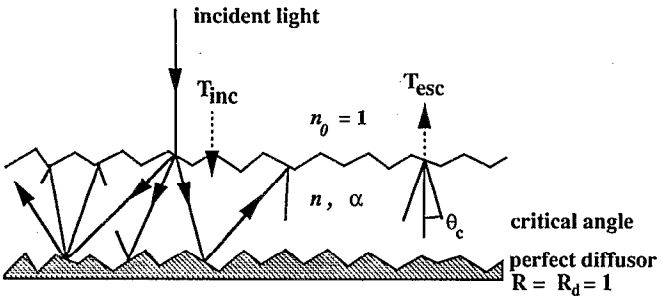

FIG. 2. Due to the interface roughness, incident light is randomly distributed in the layer. For low absorption coefficients, light is trapped in the layer because of its higher index of refraction, and hence the absorptance is enhanced.

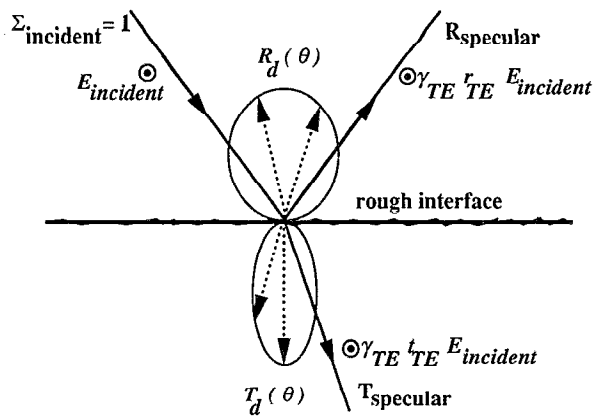

FIG. 3. Schematic illustration of the assumptions of the model for the specular and diffuse transmission and reflection of the TE mode. The same assumptions are made for the TM mode, where H replaces E.

factor $G=A/A_\perp$ (A being the absorptance in the layer and $A_\perp$ the absorptance along one orthogonal pass) reaches a maximum value G_{max} given by

$$G_{max}=4n^2\frac{T_{inc}}{T_{esc}}. \tag{10}$$

If the incident light is assumed to have an angularly uniform distribution, then $T_{inc}=T_{esc}$. Therefore, in the red part of the spectrum where $\alpha_{a\text{-Si:H}}$ tends to zero and where $n_{a\text{-Si:H}} \approx 3.7$, the maximum theoretical limit of the absorptance enhancement due to light trapping in a-Si:H solar cell is $G_{max}=4\times3.7^2\approx50$.

D. Semiempirical modeling

Because of the considerable complexity of the previously mentioned electromagnetic approaches, the most common models encountered in the literature[2–4] are based on a semiempirical treatment of light diffusion due to the TCO texture.

These models share the following common assumptions: (i) light coherence is not taken into account, preventing the prediction of interference patterns; (ii) the rough interface diffuse reflectance R_d and transmittance T_d are either experimentally determined or derived from the Mie theory, and scattering angular laws are Lambertian (cosine law); (iii) only two interfaces are assumed to be rough, the TCO/p interface and the n/back reflector interface; (iv) at a given interface, transmittance is either 1 inside the optical admittance cone, or 0 outside (i.e. total internal reflection occurs).

Because of these simplifying assumptions, light propagation through the different layers can be represented by a "mean beam." If we assume a total Lambertian diffusion, for example, this mean beam path through a layer is twice the layer thickness. Absorptances are calculated by summing the absorptances along this mean beam coming from each successive diffusion. Thus, the absorptance, written as the sum of a geometrical series, has an analytical expression. In Shade and Smith model[3,14] diffuse reflectance at the back interface (n/metal) is correlated to diffuse reflectance and transmittance at the front interface (TCO/p) according to Mie theory. Thus, the p and n layers are taken into account. In the model proposed by Morris *et al.*,[4] diffuse transmitted light is initially neglected, and the assumption of partial scattering at the back rough interface is then proposed in order to obtain a better simulation of the $Q(\lambda)$ curve.

When the back reflector exhibits a high reflectivity, these models may poorly simulate the measured $Q(\lambda)$ and $R(\lambda)$ in the red part of the visible spectrum. As discussed later, some discrepancies[4] become appearent, revealing the limits of the above-mentioned simplifying assumptions. The model we propose is also based on a semiempirical treatment of interface diffusion: Diffuse reflectance and transmittance are used as input parameters. However, specular light propagation is treated according to the rigourous plane waves equations as previously presented in the matrix method. Thus, interferential effects are taken into account, and fewer assumptions are made. Nethertheless, contrary to the models proposed by Deckman *et al.*,[2] Shade and Smith,[3] and Morris *et al.*,[4] there is no possibility of obtaining an analytical solution.

III. DESCRIPTION OF THE MODEL

A. Reflection and refraction at a rough interface

At a given rough interface, incident light is divided into two specular and two diffuse components, as shown in Fig. 3. The transverse electric (magnetic) specularly reflected and transmitted fields amplitude coefficients r'_{TE} and t'_{TE} (r'_{TM} and t'_{TM}) are assumed to be proportional to the Fresnel coefficients r_{TE} and t_{TE} (r_{TM} and t_{TM}) with a proportional factor γ_{TE} (γ_{TM}),

$$\begin{aligned} r'_{TE}&=\gamma_{TE}r_{TE} \quad (r'_{TM}=\gamma_{TM}r_{TM}),\\ t'_{TE}&=\gamma_{TE}\, t_{TE} \quad (t'_{TM}=\gamma_{TM}t_{TM}). \end{aligned} \tag{11}$$

The factor γ_{TE} (γ_{TM}), which depends on the diffuse reflectance R_d and transmittance T_d at the interface, is derived by equalizing the power flux, before and after the interface,

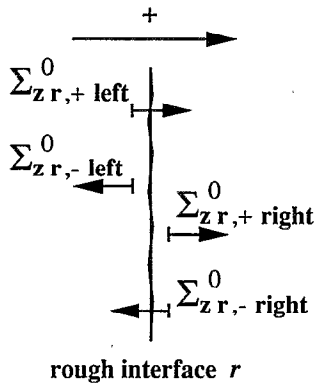

FIG. 4. Normal components of the Poynting vectors on both sides of a rough interface.

$$\text{TE:}\quad \left(1+2\frac{\mathrm{Im}(k_z)\mathrm{Im}(r_{\mathrm{TE}})}{\mathrm{Re}(k_z)}\right)\gamma_{\mathrm{TE}}^2 -2\frac{\mathrm{Im}(k_z)\mathrm{Im}(r_{\mathrm{TE}})}{\mathrm{Re}(k_z)}\gamma_{\mathrm{TE}}=1-R_d-T_d, \tag{12}$$

$$\text{TM:}\quad \left(1+2\frac{\mathrm{Im}(k_z)\mathrm{Im}(r_{\mathrm{TE}})}{\mathrm{Re}(k_z)}\right)\gamma_{\mathrm{TM}}^2 -2\frac{\mathrm{Im}(k_z)\mathrm{Im}(r_{\mathrm{TE}})}{\mathrm{Re}(k_z)}\gamma_{\mathrm{TM}}=1-R_d-T_d, \tag{13}$$

where k_z is the normal component of the incident wave vector $\mathbf{k}$. Thus, the incident light specular propagation is determined by using the matrix method with the corresponding amplitude coefficients. From the specular fields, absorptances A_m^0 in each m layer are derived.

B. Propagation of light through the multilayer stack

After determining the absorptances A_m^0 along the specular incident direction, the diffused flux must be analyzed. Each half-space surrounding the interface is sampled in several directions corresponding to an incrementation of the in-plane component k_{xy} of the wave vector $\mathbf{k}$.

At a given rough interface r, according to the previous calculation [see Eqs. (7) and (8)], the z component $\Sigma^0_{zr\mathrm{right}}$ and $\Sigma^0_{zr\mathrm{left}}$ of the specular Poynting vectors on both the right- and left-hand sides of the interface (see Fig. 4) corresponding to the specular fields are known (when the interface is smooth, due to the power conservation law, $\Sigma^0_{zr\mathrm{right}}$ and $\Sigma^0_{zr\mathrm{left}}$ are equal). For the left-hand side of the r interface (the same assumption is made for the right-hand side), in order to separate the incident flux $\Sigma^0_{zr,+\mathrm{left}}$ on the interface from the emergent flux $\Sigma^0_{zr,-\mathrm{left}}$, we assume that

$$\Sigma^0_{zr\mathrm{left}}=\Sigma^0_{zr,+\mathrm{left}}-\Sigma^0_{zr,-\mathrm{left}}, \tag{14}$$

where, in the case of the TE mode,

$$\Sigma^0_{zr,+\mathrm{left}}=\frac{1}{2\omega\mu}\left[\mathrm{Re}(k_z)|E_+|^2+\mathrm{Im}(k_z)\mathrm{Im}(E_+^*E_-)\right] \tag{15}$$

and

$$\Sigma^0_{zr,-\mathrm{left}}=\frac{1}{2\omega\mu}\left[\mathrm{Re}(k_z)|E_-|^2-\mathrm{Im}(k_z)\mathrm{Im}(E_+^*E_-)\right]. \tag{16}$$

For a nonabsorbing medium, the interferential terms in Eqs. (15) and (16) vanish, because

$$\mathrm{Im}(k_z)=0. \tag{17}$$

We have numerically verified that in the case of a typical *p-i-n* solar-cell multilayer stack, the interferential terms do not exceed 10% of the quadratic terms, allowing us to artificially separate the incident flux and the emergent flux. Thus, the specular calculations allow us to derive the incident flux $\Sigma^0_{zr,+\mathrm{left}}$ and $\Sigma^0_{zr,-\mathrm{right}}$ on each side of the rough interface r. In order to simplify our notation, $\Sigma^0_{zr,+\mathrm{left}}$ and $\Sigma^0_{zr,-\mathrm{right}}$ will be replaced by $\Sigma^0_{zr,+}$ and $\Sigma^0_{zr,-}$, respectively.

For a given k_{xy} value, we introduce the classical angular direction θ,

$$k_{xy}=\frac{2\pi}{\lambda}n\sin\theta. \tag{18}$$

The angular diffuse reflectance $R_d(\theta)$ is defined as the reflected power around the direction θ per unit solid angle. It is related to the diffuse reflectance R_d according to

$$R_d=2\pi\int_0^{\pi/2}R_d(\theta)\sin\theta\,d\theta. \tag{19}$$

Thus, the diffused reflected flux into the left-hand side in the direction θ corresponding to k_{xy} is given by

$$2\pi R_d(\theta)\sin\theta\,d\theta\,\Sigma^0_{zr,+}. \tag{20}$$

The electromagnetic field due to this "new source" is calculated in all the upper and lower layers. In each layer m, the absorptance $A_m^1(k_{xy})$ coming from this first diffusion and calculated along the k_{xy} direction is derived, as are the new incident fluxes $\Sigma^1_{zr,+}(k_{xy})$ and $\Sigma^1_{zr,-}(k_{xy})$ at rough interfaces.

Due to the phase coherence loss inherent in diffusion, absorptances $A_m^1(k_{xy})$ and incident flux on rough interfaces $\Sigma^1_{zr,+}(k_{xy})$ and $\Sigma^1_{zr,-}(k_{xy})$ in every k_{xy} direction are added in order to evaluate the total absorptance A_m^1 and the total incident flux on rough interfaces $\Sigma^1_{zr,+}$ and $\Sigma^1_{zr,-}$ due to the first diffusion:

$$A_m^1=A_m^1(0)+A_m^1(1)+\cdots+A_m^1(k_{xy})+\cdots+A_m^1(k_{xy\,\max}), \tag{21}$$

$$\Sigma^1_{zr,+}=\Sigma^1_{zr,+}(0)+\Sigma^1_{zr,+}(1)+\cdots+\Sigma^1_{zr,+}(k_{xy})+\cdots+\Sigma^1_{zr,+}(k_{xy\,\max}), \tag{22}$$

and

$$\Sigma^1_{zr,-}=\Sigma^1_{zr,-}(0)+\Sigma^1_{zr,-}(1)+\cdots+\Sigma^1_{zr,-}(k_{xy})+\cdots+\Sigma^1_{zr,-}(k_{xy\,\max}). \tag{23}$$

The new incident flux on the rough interfaces is once again diffused, and it is possible to similarly derive the absorptances A_m^2 and the new incident flux $\Sigma^2_{zr,+}$ and $\Sigma^2_{zr,-}$. The total absorptance A_m is thus given by the successive addition of each diffusion step contribution.

It is important to notice that the computation procedure is the same at the jth diffusion step to derive A_m^j, $\Sigma_{zr,+}^j$, and $\Sigma_{zr,-}^j$ from the incident flux $\Sigma_{zr,+}^{j-1}$ and $\Sigma_{zr,-}^{j-1}$. In order to take advantage of this linearity, we have developed a matrix method that greatly decreases the computation time and the effects of numerical errors. Let us first define the column vectors $\{A_m^j\}$ and $\{\Sigma_{zr,\pm}^j/\Sigma_z^{\text{inc}}\}$ (fluxes are normalized to the incident flux Σ_z^{inc} in order to have homogeneous variables A_m and $\Sigma_{zr,\pm}^j/\Sigma_z^{\text{inc}}$):

$$\{A_m^j\}=\begin{pmatrix} A_0^j \\ A_1^j \\ \cdots \\ A_m^j \\ \cdots \\ A_{M-1}^j \end{pmatrix}_{M \text{ layers}}, \qquad \left\{\frac{\Sigma_{zr,\pm}^j}{\Sigma_z^{\text{inc}}}\right\}=\frac{1}{\Sigma_z^{\text{inc}}}\begin{pmatrix} \Sigma_{z1,+}^j \\ \Sigma_{z1,-}^j \\ \Sigma_{zr,+}^j \\ \Sigma_{zr,-}^j \\ \Sigma_{zR,+}^j \\ \Sigma_{zR,-}^j \end{pmatrix}_{R_{\text{interfaces}}^{\text{rough}}} \tag{24}$$

The superscript j indicates that the parameters are related to the jth diffusion step. $\{A_m^j\}$ has M elements ($M-2$ is the number of layers in the stack, and the index 0 refers to the incident medium, whereas index $M-1$ refers to the emergent medium), $\{\Sigma_{zr,\pm}^j/\Sigma_z^{\text{inc}}\}$ has $2\times R$ elements (R is the number of rough interfaces and both $+$ and $-$ directions are taken into account). In order to use the linearity in the computation process, we introduce the following $[A]$ and $[F]$ matrices:

$$\{A_m^j\}=[A]\{\Sigma_{zr,\pm}^{j-1}/\Sigma_z^{\text{inc}}\}, \tag{25}$$

$$\{\Sigma_{zr,\pm}^j/\Sigma_z^{\text{inc}}\}=[F]\{\Sigma_{zr,\pm}^{j-1}/\Sigma_z^{\text{inc}}\}. \tag{26}$$

Each successive contribution can be expressed as a function of the specular normalized flux incident on the rough interfaces $\{\Sigma_{zr,\pm}^0/\Sigma_z^{\text{inc}}\}$,

$$\{A_m^j\}=[A][F]\{\Sigma_{zr,\pm}^{j-2}/\Sigma_z^{\text{inc}}\}=[A][F]^{j-1}\{\Sigma_{zr,\pm}^0/\Sigma_z^{\text{inc}}\}. \tag{27}$$

The total diffuse absorptance $\{A_m^{\text{diff}}\}$, meaning the absorptance due to scattering, is given by

$$\begin{aligned}\{A_m^{\text{diff}}\}&=\{A_m^1\}+\{A_m^2\}+\cdots+\{A_m^j\}+\cdots \\ &=[A]([F]^0+[F]^1+\cdots+[F]^{j-1}+\cdots) \\ &\quad\times\{\Sigma_{zr,\pm}^0/\Sigma_z^{\text{inc}}\}.\end{aligned} \tag{28}$$

Thus, [Id] being the identity matrix, it is easy to derive $\{A_m^{\text{diff}}\}$,

$$\{A_m^{\text{diff}}\}=[A]([\text{Id}]-[F])^{-1}\{\Sigma_{zr,\pm}^0/\Sigma_z^{\text{inc}}\}, \tag{29}$$

and the total absorptance $\{A_m\}$ is the sum of the specular and diffuse components,

$$\{A_m\}=\{A_m^0\}+\{A_m^{\text{diff}}\}. \tag{30}$$

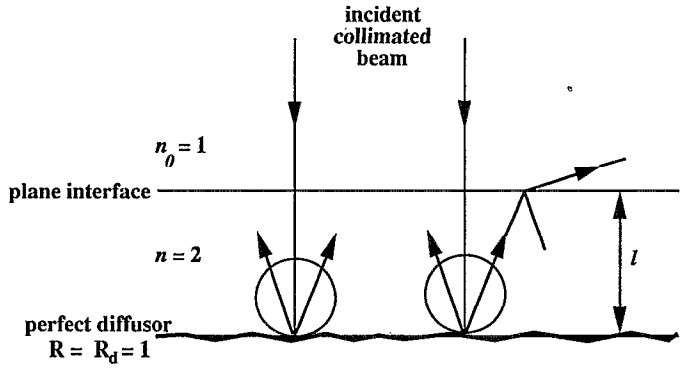

FIG. 5. Ideal test structure to verify the light trapping thermodynamic limit.

In practice, $\{A_m^0\}$ and $\{\Sigma_{zr,\pm}^0/\Sigma_z^{\text{inc}}\}$ are first calculated, and the $[A]$ and $[F]$ matrices are determined when calculating $\{A_m^1\}$ and $\{\Sigma_{zr,\pm}^1/\Sigma_z^{\text{inc}}\}$ following the procedure described at the beginning of this subsection.

C. Input parameters

Considering Fig. 1, showing the multilayer structure of a typical *p-i-n* solar cell, we see that there are four rough interfaces. However, due to the low p- and n-layer thicknesses in comparison to the texture feature size, it is justified to consider that the p/i and i/n interfaces are optically flat. Thus, we have assumed that in *p-i-n* solar cells, only two interfaces are rough, namely the TCO/p (front) and n/back reflector (back) interfaces. Another simplifying assumption is that diffusion is symmetrical between two adjacent m and $m+1$ layers,

$$\begin{aligned}R_{d,m+1/m}&=R_{d,m/m+1}, \\ T_{d,m+1/m}&=T_{d,m/m+1}.\end{aligned} \tag{31}$$

Thus, at a given incident wavelength λ, the optical effects of the TCO texture in the stack are modeled by four parameters: the diffuse reflectances $R_{d\ \text{front}}$, $R_{d\ \text{back}}$ and the diffuse transmittances $T_{d\ \text{front}}$, $T_{d\ \text{back}}$. These coefficients have been experimentally derived at selected wavelengths.

Due to the high index of refraction of the a-Si:H layer, the sampling interval for the space variable $k_{xy}(\lambda/2\pi)$ has been fixed to [0,4] with an increment step equal to 0.1. Therefore, the number of directions in the air is 10 but reaches 40 in the a-Si:H layer.

IV. NUMERICAL VERIFICATION OF THE THERMODYNAMIC LIGHT-TRAPPING LIMIT

After the usual testing on plane interface structures and in order to evaluate the effects of numerical errors on the final accuracy, we have numerically verified the thermodynamic light trapping limit. Let us consider a layer of an absorbing medium (see Fig. 5) having a complex index of refraction $\tilde{n}=n+i\kappa$ and with a thickness l. The front interface is assumed to be flat, whereas the back interface is assumed to be an ideal reflector and diffusor. The incident beam is collimated and normal to the layer.

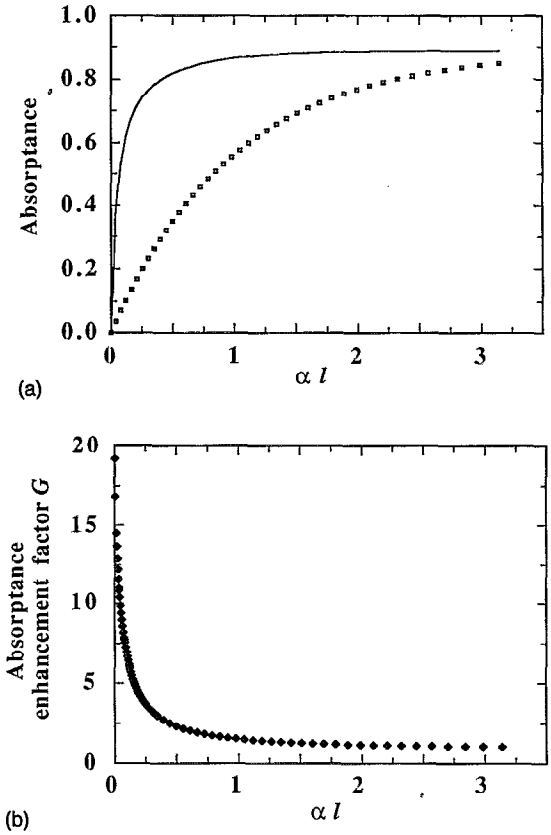

FIG. 6. (a) Calculated absorptance in the medium of index $n=2$ (cf. Fig. 5) as a function of αl for a perfectly absorbing (square dots, $R_d=0$) and a perfectly reflecting (solid line curve, $R_d=1$) diffusive back contact. (b) Absorptance enhancement factor G [ratio of absorptances of (a)] as a function of αl.

We have studied the variations of the absorptance A as a function of αl, for $\alpha l \ll 1$. n was taken to be 2 for the numerical test. The mean power transmission coefficients T_{inc} and T_{esc} at the front interface have been calculated[5,7] according to

$$T_{\text{inc}}=\frac{n}{n_{\text{air}}}|t_{\text{TE}}|^2=\frac{n_{\text{air}}}{n}|t_{\text{TM}}|^2 \quad (\text{at } k_{xy}=0), \tag{32}$$

$$T_{\text{esc}}=\left(\frac{n}{n_{\text{air}}}\right)^2\int_0^{\theta_c}\left(\frac{n}{n_{\text{air}}}|t_{\text{TE}}|^2+\frac{n_{\text{air}}}{n}|t_{\text{TM}}|^2\right)\times\cos\theta\sin\theta\,d\theta. \tag{33}$$

When the medium becomes less and less absorbing, according to the light-trapping limit, the enhancement factor G reaches the maximum value

$$G_{\max}=4n^2\frac{T_{\text{inc}}}{T_{\text{esc}}}=19.35. \tag{34}$$

We present in Fig. 6(a) the calculated absorptances for different αl values. When αl is low, absorptance $A_\perp$ for one normal pass is close to αl. As we can see in Fig. 6(b), the ratio $A/A_\perp$ tends to 19.2 when αl tends to zero, which is in very good agreement with the theoretical $G_{\max}$ value. Thus, the numerical algorithm permits us to decrease the computation time while keeping numerical accuracy.

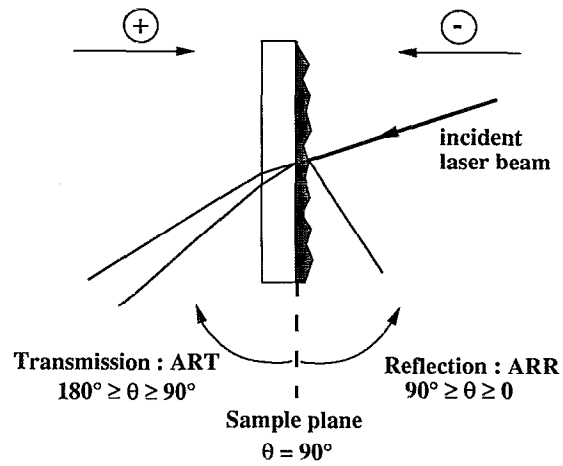

FIG. 7. Chosen conventions for the ARR and ART measurements.

V. EXPERIMENTAL DETERMINATION OF THE SCATTERING COEFFICIENTS

A. Experimental setup

The experimental setup consists of a crystalline silicon detector placed on a rotating arm. The light source is a chopped krypton laser beam, alternatively tuned at the four following emitting wavelengths: 472, 568, 647, and 752 nm. A lock-in amplifier is used to extract the sensor signal. By measuring the signal corresponding to the incident beam flux (provided that the sensor active area is larger than the incident beam diameter), it is possible to derive[14] the normalized diffuse angular-resolved-reflectance (ARR) or -transmittance (ART). The scheme presented on Fig. 7 shows the notation we have chosen.

B. Samples

Two types of TCO substrates have been studied. The main characteristics of the substrates are summarized in Table I. Absorptances of the bare TCO substrates placed in ethanol are measured by the use of photothermal deflexion spectroscopy (PDS), the PDS spectra being calibrated by making use of the joule heating inside the films.[15] TCO texture is analyzed by the scanning electron microscopy (SEM) technique.

The TCO substrates are covered either with aluminum or with a-Si:H. Thus, optical diffusion properties of the TCO/air, TCO/a-Si:H, and TCO/aluminum interfaces have been investigated and compared.

TABLE I. Main characteristics of the TCO substrates nos. 1 and 2.

TCO substrate	1	2
Glass thickness	1.1 mm	2 mm
TCO thickness	700 nm	1200 nm
Mean roughness feature size	170 nm	300 nm
TCO square sheet resistance	6.5 Ω/□	9 Ω/□
TCO total absorptance (AM1.5)	6.9%	5.3%
Haze ratio H_r at 633 nm	7%	13%

TABLE II. Summary of angular-resolved-reflectance (ARR) and -transmittance (ART) measurements achieved on different polished structures. +(−) refers to an incident light coming from the glass substrate (polished surface) side. Structures are polished in order to independently analyze the diffusion properties of the front and the back rough interfaces.

Structures	472 nm	568 nm	647 nm	752 nm
TCO1/*a*-Si:H (18 μm) polished	ARR+	ARR+	ARR+	ARR+,− ART+,−
TCO2/*a*-Si:H (7 μm) polished	ARR+	ARR+	ARR+	ARR+,− ART+,−
TCO1/Al (150 nm)/ *a*-Si:H (7 μm) polished			ARR−	ARR−
TCO2/Al (150 nm)/ *a*-Si:H (7 μm) polished			ARR−	ARR−

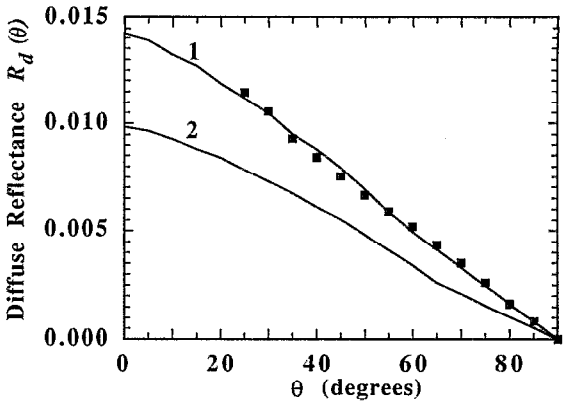

FIG. 9. Same as in Fig. 8, with two linear diffuse reflectance laws $R_d(\theta)$ and different total reflectance R_d. Curve 1: $R_d=13\%$; curve 2: $R_d=10\%$.

In the case of the *a*-Si:H-covered samples, in order to derive the diffusion properties of the front and back rough interfaces separately, thick *a*-Si:H layers are deposited either on the bare TCO films (front interface) or on a 2000-Å-thick aluminum layer previously deposited on the TCO films (back interface). Free *a*-Si:H surfaces are then polished, as summarized in Table II. This polishing is achieved by using a granular diamond paste. Thus, the resulting stacks have only one rough interface, which makes the analysis easier. In the near-infrared region, TCO/*a*-Si:H samples have been irradiated from both the + and − sides. Moreover, assuming that the 2000-Å-thick aluminum layer conformally covers the TCO texture, and that the aluminum/*a*-Si:H interface scattering properties do not depend on the deposition order, the back interface diffuse reflectance is also investigated.

C. Results

1. Angular-resolved reflectance and transmittance

As a general result, ARR measurements for both TCO roughness and for each interface present a mostly linear angular dependence. The experimental ARR and ART angular dependence does not demonstrate any structure or any resonance. Similar results have been reported by Shade and Smith.[14]

In Figs. 8 and 9, the solid line curves correspond to simulated ARR curves for the entire stack, obtained for different angular diffusion laws $R_{d\ \mathrm{front}}(\theta)$ at the front interface, and square dots correspond to the measured ARR at the incident wavelength 472 nm. The experimental angular dependencies can be approximated by using a linear law, but cosine laws to the power 1 or 2 could also be used, as shown in Fig. 8. In order to show the effect of the total diffuse reflectance $R_{d\ \mathrm{front}}$, we present in Fig. 9 results for two different values of $R_{d\ \mathrm{front}}$.

At the near-infrared wavelength 752 nm, ARR and ART measurements obtained when irradiating from both sides are shown in Fig. 10, where solid line curves correspond to simulated values.

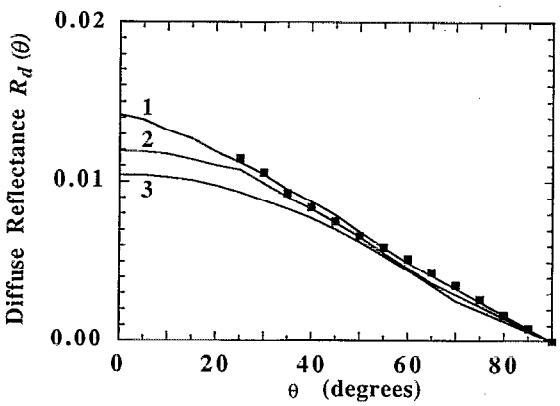

FIG. 8. Measured (square dots) and simulated (solid line curves) ARR for the glass/TCO1/*p* ($l_p=8$ nm)/*i* ($l_i=18$ μm) structure, at $\lambda=472$ nm. Curve 1: $R_d(\theta)$ is linear with a total reflectance $R_d=13\%$. Curve 2: $R_d(\theta)$ is proportional to $\cos^2\theta$ with $R_d=10\%$. Curve 3: $R_d(\theta)$ is Lambertian (cosine law) with $R_d=14\%$.

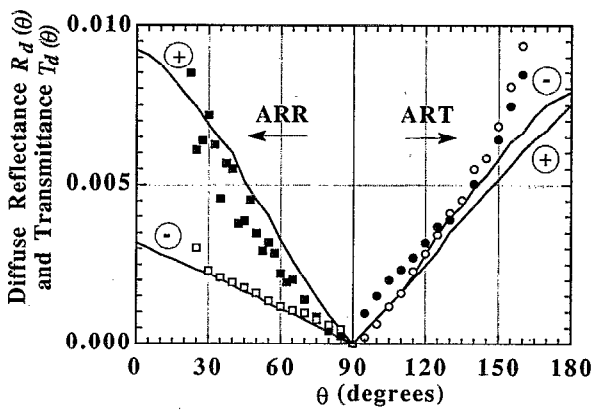

FIG. 10. Measured (points) and simulated (solid line curves) ARR and ART measurements at $\lambda=752$ nm for the glass/TCO1/*p*/*i* ($l_i=7$ μm) stack, after polishing of the *i* layer surface. For the simulations, both $R_d(\theta)$ and $T_d(\theta)$ at the rough TCO1/*p* interface are assumed to be symmetrical, and therefore are the only free parameters.

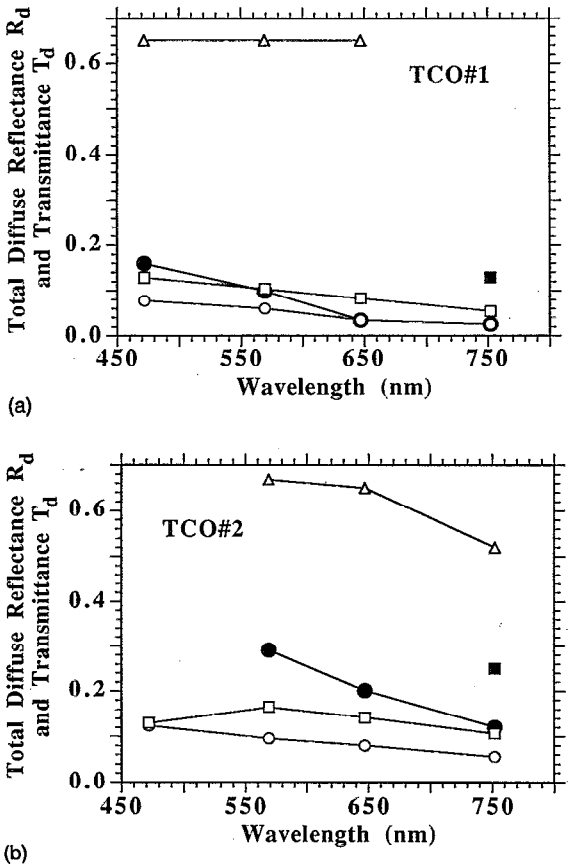

FIG. 11. (a) Spectral dependence of the diffuse reflectance R_d and transmittance T_d for the TCO1/air (—○—: R_d; —●—: T_d), the TCO1/a-Si:H (—□—: R_d; —■—: T_d), and the TCO1/Al (—△—: R_d) interfaces. (b) Spectral dependence of the diffuse reflectance R_d and transmittance T_d for the TCO2/air (—○—: R_d; —●—: T_d), the TCO2/a-Si:H (—□—: R_d; —■—: T_d), and the TCO2/Al (—△—: R_d) interfaces.

2. Spectral dependence of diffuse reflectance and transmittance

When simulating as closely as possible each of the experimental curves by using different angular diffusion laws $R_{d\ \mathrm{front}}(\theta)$, $T_{d\ \mathrm{front}}(\theta)$, $R_{d\ \mathrm{back}}(\theta)$, and $T_{d\ \mathrm{back}}(\theta)$, the total diffuse reflectance R_d and transmittance T_d for each interface and for the four wavelengths are estimated [see Eq. (19)].

We present in Fig. 11 the spectral variation of the R_d coefficients for the TCO/air, TCO/a-Si:H, and TCO/aluminum interfaces, for two different TCO roughnesses, TCO1 and TCO2.

For both TCO roughnesses the diffuse reflectance R_d is the lowest for the bare TCO layers, and the highest for the TCO/aluminum interfaces. R_d in the air is higher for the most textured (TCO2) substrate, and it increases with decreasing incident wavelength. This wavelength dependence, still valid for the moderately textured TCO1/a-Si:H interface, is not found anymore for the TCO2/a-Si:H interface, where R_d reaches a maximum value at 568 nm. The former spectral dependence can be related to Raylcigh scattering, whereas the latter may signify Mie scattering, as reported by O'Dowd.[13] For the TCO/aluminum interface R_d is about the same for both substrates, and it seems to saturate at a value of 65%. Such a saturation effect has been reported by Shade and Smith[14] when calculating, according to Mie theory, the scattering properties of silver particles in air.

ART measurements show that T_d is higher than R_d for the TCO/air and TCO/a-Si:H interfaces. For the TCO/air interface, the increase of T_d with decreasing incident wavelength is also higher than that of R_d.

For the back n/Al rough interface, the experimentally derived $R_{d\ \mathrm{front}}$ diffuse reflectance is about 60% for TCO1 and 40% for TCO2 at an incident wavelength of 752 nm. The ARR measurements are not very accurate, since a remaining parasitic reflectance at the polished air/a-Si:H interface can make a non-negligible contribution to the total reflectance.

3. Conclusion

We have experimentally observed that the diffusion properties of the TCO/layer m interface strongly depends on the refraction index of layer m. The TCO1/air and TCO2/air interfaces are respectively moderately and very rough, whereas the TCO1/Al and TCO2/Al interfaces show the same diffuse reflectance. Moreover, according to the experimentally determined diffuse reflectance of the TCO/a-Si:H interfaces, it seems that the TCO roughness effects on actual solar cells optical properties are not directly linked to spectrophotometric measurements achieved on bare substrates. This might be related to the fact that several studies (see, for example, Gordon *et al.*[16]) have reported a saturation in the solar-cell conversion efficiency improvement when increasing the TCO diffuse transmittance. According to Mie theory, the dominating factor is the ratio of the texture feature size to the wavelength in the material, as reported by Shade and Smith[14] by comparing the diffusion coefficients of silver spheres and the same TCO spheres in air.

VI. NUMERICAL SIMULATION OF THE OPTICAL ABSORPTANCES IN SOLAR CELLS

A. Quantum spectral response of devices deposited on a moderately rough TCO substrate

We have deposited two p-i-n structures on the TCO1 substrate, covered with two different back metallizations. The first stack consists of TCO1/l_p=8 nm/l_i=320 nm/l_n=40 nm/Al. We present in Fig. 12 the experimental $Q(\lambda)$ and simulated absorptances in the i layer, obtained for different diffuse reflectances and transmittances.

At wavelengths lower than 600 nm, due to the high a-Si:H absorption coefficient, only the front interface need be taken into account. If we use the derived spectral $R_{d\ \mathrm{front}}$ diffuse reflectance and a low $T_{d\ \mathrm{front}}$ diffuse transmittance, the simulated $Q(\lambda)$ is lower than the experimental value, and it shows a larger interferential effect. Since the $T_{d\ \mathrm{front}}$ value can not be experimentally derived, we have assumed that $T_{d\ \mathrm{front}}$ is much larger than the

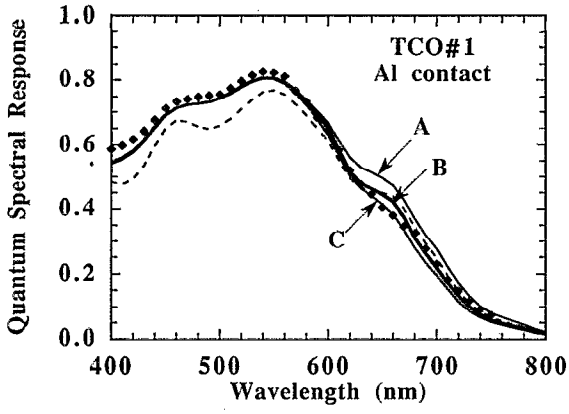

FIG. 12. Measured (square dots) and simulated (solid and dashed-line curves) $Q(\lambda)$ for a glass/TCO1/*p-i-n*/Al solar cell. $R_{d\ \mathrm{front}}$ values are the experimentally derived values [see Fig. 11(a)]. Dashed line: $T_{d\ \mathrm{front}}$ assumed to have the same spectral variation as $R_{d\ \mathrm{front}}$ solid line curves: $T_{d\ \mathrm{front}} = 80\%$ at 400 nm, and $T_{d\ \mathrm{front}} = 50\%$ at 800 nm, with a linear $T_{d\ \mathrm{front}}(\lambda)$ spectral law. $T_{d\ \mathrm{front}}(\theta)$ is assumed to be proportional to $\cos^3\theta$. At the back rough interface, $R_{d\ \mathrm{back}}(\theta)$ and $T_{d\ \mathrm{back}}(\theta)$ are assumed to be Lambertian, with different $R_{d\ \mathrm{back}}$ and $T_{d\ \mathrm{back}}$ values. Curve A: $R_{d\ \mathrm{back}} = 60\%$, $T_{d\ \mathrm{back}} = 40\%$; curve B: $R_{d\ \mathrm{back}} = 40\%$, $T_{d\ \mathrm{back}} = 40\%$; curve C: $R_{d\ \mathrm{back}} = 60\%$, $T_{d\ \mathrm{back}} = 60\%$.

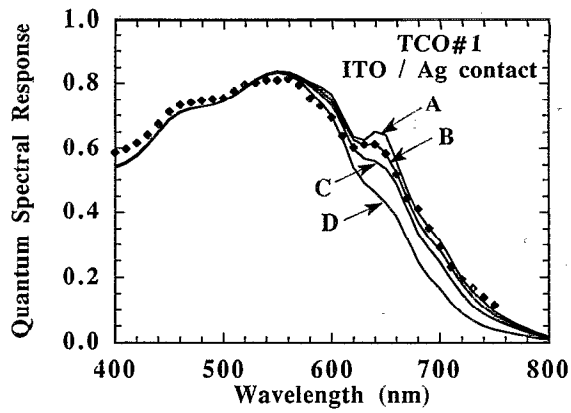

FIG. 13. $Q(\lambda)$ for the same solar cell as in Fig. 12, with an ITO ($l_{\mathrm{ITO}}=5$ nm)/Ag back contact. $R_{d\ \mathrm{front}}$ and $T_{d\ \mathrm{front}}$ are the same as in Fig. 12, on curves A, B, and C. Curve A: $R_{d\ \mathrm{back}} = 40\%$, $T_{d\ \mathrm{back}} = 10\%$; curve B: $R_{d\ \mathrm{back}} = 40\%$, $T_{d\ \mathrm{back}} = 20\%$; curve C: $R_{d\ \mathrm{back}} = 40\%$, $T_{d\ \mathrm{back}} = 40\%$; curve D: $R_{d\ \mathrm{back}} = 0\%$, $T_{d\ \mathrm{back}} = 100\%$ (no light reflected at the ITO/Ag interface).

$R_{d\ \mathrm{front}}$ value. For all the following simulations on TCO1, $R_{d\ \mathrm{front}}$ is the same as previously derived, and $T_{d\ \mathrm{front}}$ is 80% at 400 nm and 50% at 800 nm.

These high values of the diffuse transmittance are related to the texture effect at the TCO/*p* interface: Due to the large grain size and by analogy with effective media theory, the transmittance is higher since the interface is no longer optically abrupt. In order to take into account this phenomenon (previously reported by Walker *et al.*[17] and other groups), we have chosen an angular dependence law varying as a $\cos^3$ function, which is more centered around the normal direction.

The rough front interface R_d and T_d being determined, we present in Fig. 12 three simulated $Q(\lambda)$ curves obtained for different $R_{d\ \mathrm{back}}$ and $T_{d\ \mathrm{back}}$ values. For $R_{d\ \mathrm{back}} = 40\%$ (60%) and $T_{d\ \mathrm{back}} = 60\%$ (40%), light diffusion is complete at the back interface, whereas for $R_{d\ \mathrm{back}} = T_{d\ \mathrm{back}} = 40\%$, 20% of the light remains specularly reflected and refracted at the back rough interface. These values of $R_{d\ \mathrm{back}}$ are in good agreement with the value experimentally determined (i.e., $R_{d\ \mathrm{back}} \approx 40\%$). The experimental and the calculated $Q(\lambda)$ curves present a vanishing bump around 650 nm, which corresponds to an interferential effect occuring in the TCO layer. It does not occur in the *i* layer since it is observable even when diffusion is complete at the back interface.

The second stack consists of TCO1/l_p=8 nm/l_i=460 nm/l_n=30 nm/ITO(l_{ITO}=5 nm/Ag. We present in Fig. 13 the experimental $Q(\lambda)$ and simulated absorptances in the *i* layer obtained for different $R_{d\ \mathrm{back}}$ and $T_{d\ \mathrm{back}}$ values. The back rough interface is assumed to be the ITO/Ag interface, the *n*/ITO interface being flat. A bump clearly becomes appearent around 640 nm, narrower than the previous one (see Fig. 12). This second bump is associated with an interferential effect in the *i* layer, which is enhanced by the low index of the ITO layer. The best fit is obtained when taking $R_{d\ \mathrm{back}} = 40\%$ and $T_{d\ \mathrm{back}} = 20\%$. In order to show the benefit of the back ITO/Ag reflection, we report the calculated absorptance corresponding to $R_{d\ \mathrm{back}} = 0\%$ and $T_{d\ \mathrm{back}} = 100\%$. In this case, no light, either specular or diffuse, is back reflected at the ITO/Ag interface.

We have also calculated the *i* layer absorptance for a thicker ITO back layer (l_{ITO}=60 nm), keeping the other parameters constant. The short-circuit current integrated over the AM1.5 spectrum increases from 13.1 to 13.5 mA/cm^2.

B. Total reflectance and quantum spectral response of devices deposited on very rough TCO substrates

With the use of our numerical program, we have analyzed the experimental $R(\lambda)$ and $Q(\lambda)$ curves published by Morris *et al.*[4] Different *p-i-n* structures (l_p=12 nm/l_i=525 nm/l_n=30 nm) are deposited on a TCO substrate ("TCO M") with $l_{\mathrm{TCO\ M}}$=650 nm, and four back reflectors are used.

Due to the absence of interferential pattern in the experimental spectra, we infer that the TCO M roughness is very high. In order to analyze the diffuse reflectance and transmittance of the front rough interface and to verify the refraction index values, we first study a stack with a very poor back reflector (molybdenum reflector). Between 400 and 600 nm, the reported experimental $Q(\lambda)$ exhibits a very high value, as shown in Fig. 14. In order to account for this high value, it is necessary to increase $T_{d\ \mathrm{front}}$. For the following computations, we assume that $R_{d\ \mathrm{front}}$ is the same as previously measured with the very rough TCO2, and that $T_{d\ \mathrm{front}}$ is such that

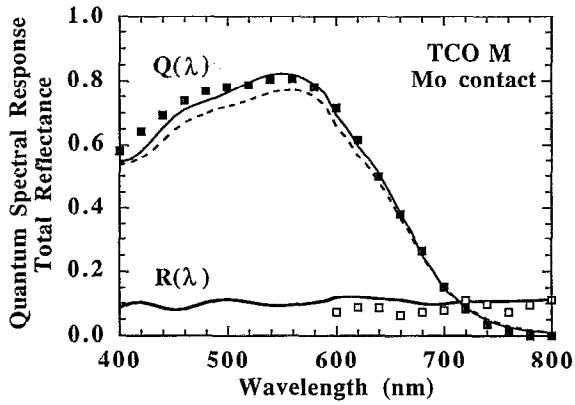

FIG. 14. Measured [square dots: from Morris *et al.* (Ref. 4)] and simulated (solid line curves) $Q(\lambda)$ and $R(\lambda)$ for a glass/TCO M/*p-i-n*/Mo solar cell. For the front rough interface, $R_{d\ \mathrm{front}}$ has the same value as for TCO2 (very rough TCO substrate), and $T_{d\ \mathrm{front}} = 0.95 - R_{d\ \mathrm{front}}$. Solid line curve: κ_{TCO} used in the simulation is derived from PDS measurement performed on TCO2. Dashed line: κ_{TCO} is given by Morris *et al.* (Ref. 4).

$$T_{d\ \mathrm{front}} = 0.95 - R_{d\ \mathrm{front}}. \tag{35}$$

For the computed simulations, we use the same indices of refraction as the values given by the authors of Ref. 4. However, when using the TCO M extinction coefficient κ values given by the authors, it becomes appearent that the $Q(\lambda)$ calculated values underestimate the experimental data, as shown in Fig. 14. TCO thin films show low absorption levels over the visible spectrum, and it is usually difficult to measure κ. According to the photothermal deflection technique we have developed,[15] lower extinction coefficient values are derived compared to the abovementioned values. Due to the fact that a better fit is obtained, we choose to use the κ values derived by PDS on TCO2. Eventually, we assume that TCO M and TCO2 have the same diffuse reflectance and the same index of refraction, but different thickness.

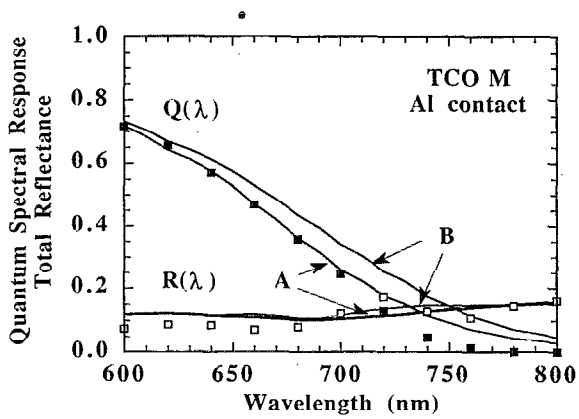

FIG. 15. Measured [square dots: from Morris *et al.* (Ref. 4)] and simulated $Q(\lambda)$ and $R(\lambda)$ for the same solar cell as in Fig. 14, with an Al back contact. $R_{d\ \mathrm{front}}$ and $T_{d\ \mathrm{front}}$ are the same as in Fig. 14. Curve A: $R_{d\ \mathrm{back}} = 25\%$, $T_{d\ \mathrm{back}} = 65\%$; curve B: $R_{d\ \mathrm{back}} = 40\%$, $T_{d\ \mathrm{back}} = 60\%$.

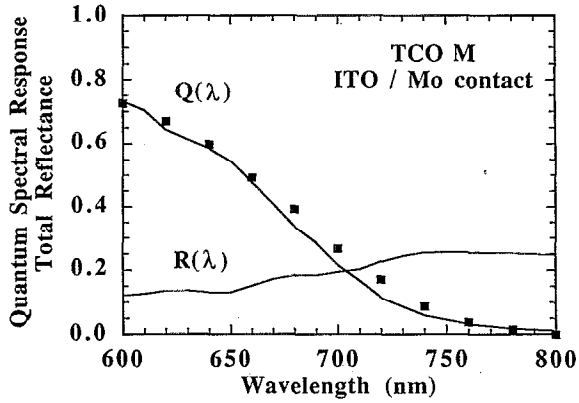

FIG. 16. Measured [square dots: from Morris *et al.* (Ref. 4)] and simulated $Q(\lambda)$ for the same solar cell as in Fig. 14, with an ITO/Mo back contact. $R_{d\ \mathrm{back}} = 20\%$, $T_{d\ \mathrm{back}} = 70\%$.

In the case of the Mo metallization, both simulated $Q(\lambda)$ and $R(\lambda)$ curves are in good agreement with the experimental curves when using $R_{d\ \mathrm{back}} = 6\%$ and $T_{d\ \mathrm{back}} = 92\%$. For the other back metallizations, we only change the values of $R_{d\ \mathrm{back}}$ and $T_{d\ \mathrm{back}}$, keeping all the other parameters constant.

For the three other back metallizations, experimental $Q(\lambda)$ and $R(\lambda)$ curves are compared to calculated curves for different $R_{d\ \mathrm{back}}$ and $T_{d\ \mathrm{back}}$ values, as shown in Figs. 15–17. For the aluminum (ITO/Mo) back contact, a good agreement is obtained when $R_{d\ \mathrm{back}} = 25\%$ and $T_{d\ \mathrm{back}} = 65\%$ ($R_{d\ \mathrm{back}} = 20\%$ and $T_{d\ \mathrm{back}} = 70\%$). As mentioned by Morris *et al.*,[4] the ITO/Ag back contact is the most interesting case since it strongly reflects the incident light. A fairly good agreement is obtained when using $R_{d\ \mathrm{back}} = 70\%$ and $T_{d\ \mathrm{back}} = 25\%$. We report in Fig. 17 the simulated $Q(\lambda)$ and $R(\lambda)$ curves in the case of a perfect diffusor (i.e., $R_{d\ \mathrm{back}} = 100\%$ and $T_{d\ \mathrm{back}} = 0\%$).

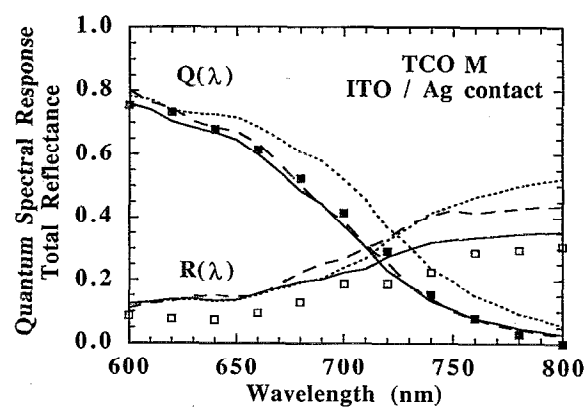

FIG. 17. Measured [square dots: from Morris *et al.* (Ref. 4)] and simulated $Q(\lambda)$ and $R(\lambda)$ for the same solar cell as in Fig. 14, with an ITO/Ag back contact. Solid line curve: $R_{d\ \mathrm{back}} = 70\%$, $T_{d\ \mathrm{back}} = 25\%$; long-dashed line: $R_{d\ \mathrm{back}} = 40\%$, $T_{d\ \mathrm{back}} = 20\%$; short-dashed line: $R_{d\ \mathrm{back}} = 100\%$, $T_{d\ \mathrm{back}} = 0\%$ (perfect diffusor).

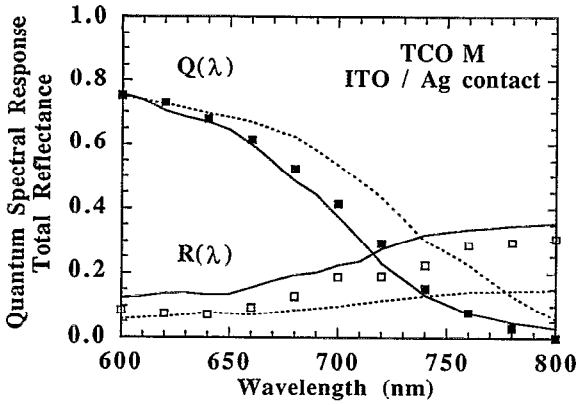

FIG. 18. Same as in Fig. 17. Solid line curve: $R_{d\ \mathrm{back}} = 70\%$, $T_{d\ \mathrm{back}} = 25\%$; dashed line: from the model of Morris *et al.* (Ref. 4).

VII. DISCUSSION

A. Comparison between previous semiempirical model and present model

As mentioned by Morris *et al.*,[4] both $Q(\lambda)$ and $R(\lambda)$ curves must be taken into account in order to model the optical properties of *a*-Si:H solar cells. The back diffuse reflectance and transmittance experimentally determined by the authors and used as input parameters of their analytical modeling are very close to the values we used in order to fit the experimental curves. Thus, apart from the light propagation treatment and the TCO extinction coefficient κ, the input parameters of the two models are approximately similar.

When using the model of Morris *et al.*,[4] the simulated $Q(\lambda)$ and $R(\lambda)$ curves for the ITO/Ag back metallization respectively overestimate and underestimate the experimental curves (see Fig. 18). As mentioned by the authors, any attempt to reduce the computed $Q(\lambda)$ values leads to a decrease in the corresponding $R(\lambda)$ values which cannot reconcile with experimental observations and demonstrates the limitation of their modeling. Figure 18 shows that a better fit is obtained between the experimental and simulated optical characteristics when using our modeling. This improvement mainly comes from a better treatment of the specular light propagation through the multilayer stack.

B. Optical loss in the TCO layer

One of the main aims of the *a*-Si:H solar-cell optical analysis is to evaluate the optical loss in the front transparent electrode. The usual TCO thin-film qualification consists in measuring the optical specular and diffuse transmittances of bare TCO substrates and tentatively relating these characteristics to the optical properties of the cell. The model we have proposed allows an accurate estimation of the potential enhancement of the cell short-circuit current density J_{sc} that may arise from an ideal optimization of the TCO optical transparency. In order to calculate this enhancement, we introduce for two TCO substrates (TCO1 and TCO M) a corresponding ideal substrate having the same film thickness, the same topology and hence

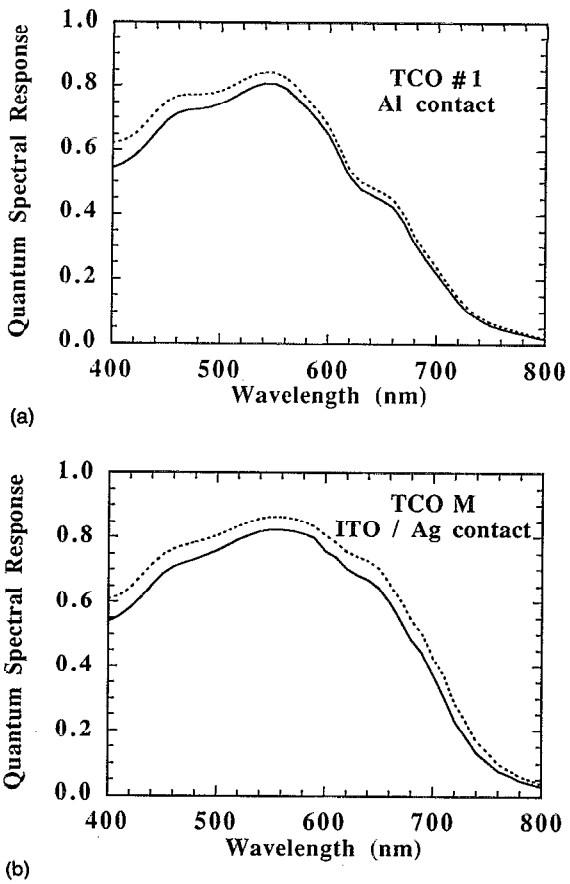

FIG. 19. Effect of TCO absorption losses on the quantum spectral response of a solar cell for two different cell structures. (a) glass/TCO1/*p-i-n*/Al. Solid line curve: same $Q(\lambda)$ as in Fig. 12 (curve B); dashed line: $\kappa_{\mathrm{TCO1}}=0$ (ideal TCO1 transparency). (b) Glass/TCO M/*p-i-n*/ITO/Ag. Solid line curve: same as in Fig. 17 (solid line curve); dashed line: $\kappa_{\mathrm{TCO\ M}}=0$ (ideal TCO M transparency).

the same interface diffuse reflectances and transmittances, and the same real index of refraction. The extinction coefficient κ_{TCO} is artificially put to zero, and the same computations as before (i.e., with the same *p-i-n* structures and back metallizations) are performed in order to compare the $Q(\lambda)$ curves (see Fig. 19). For four of the previously studied structures, we also present in Table III the calculated integrated short-circuit current density J_{sc} and the increase ΔJ_{sc} that would be expected from an optimized TCO transparency. ΔJ_{sc} increases with the TCO roughness and with the back contact reflectivity. For the roughest TCO and for the ITO/Ag back contact, ΔJ_{sc} reaches the maximum value 1.16 mA/cm^2. For the aluminum back

TABLE III. Short-circuit integrated current density J_{sc} (mA/cm^2) and increase ΔJ_{sc} calculated by comparing the simulated quantum spectral response $Q(\lambda)$ of realistic cells and of identical cells deposited on a perfectly nonabsorbing (ideal) TCO substrate.

	Moderately rough TCO (TCO1)			Very rough TCO (TCO M)		
	J_{sc}	ΔJ_{sc}	$\Delta J_{sc}/J_{sc}$	J_{sc}	ΔJ_{sc}	$\Delta J_{sc}/J_{sc}$
Al	11.98	0.72	6%	12.82	0.95	7.4%
ITO/Ag	13.10	1.06	8.1%	13.89	1.16	8.4%

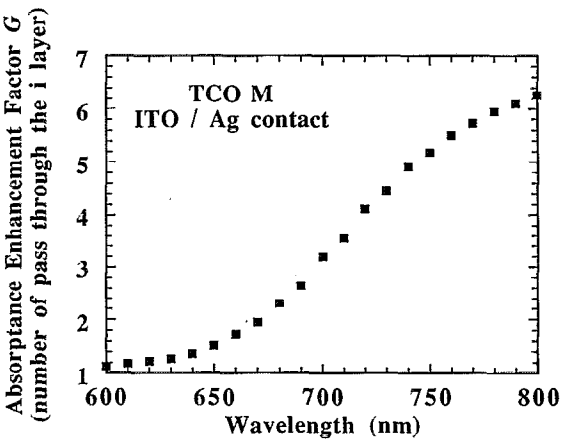

FIG. 20. i layer absorptance enhancement factor G calculated for the most efficient solar cells (TCO M and ITO/Ag back contact). For low αl values, G represents the equivalent number of orthogonal light passes through the i layer.

electrode, it is noticeable that ΔJ_{sc} is lower in the red part of the visible spectrum, and thus that the main benefit occurs at short wavelengths. Due to the a-Si:H/Al interface absorption, light trapping for red light is limited by the back electrode absorption, and a poor enhancement is expected from the TCO transparency optimization. For the ITO/Ag back contact, ΔJ_{sc} is the same at wavelengths $\leqslant$600 nm because of the high absorption of a-Si:H in this region; however, ΔJ_{sc} is higher in the red part of the spectrum, where light trapping is more efficient.

Our computations demonstrate that the highest benefit is obtained when using rough TCO substrates and highly reflecting back contacts. For a moderately rough TCO substrate and aluminum back electrode, the light trapping efficiency and hence ΔJ_{sc} are limited by the back contact's poor reflectivity.

C. Maximum number of equivalent passes through the active layer

Comparing the calculated i layer absorptance to the absorptance $A_\perp$ for one orthogonal pass allows us to derive the absorptance enhancement factor G, which corresponds for low αl values to the number of equivalent passes through the active layer. In order to calculate $A_\perp$, we assume that the back layer is a perfect absorber. Figure 20 shows the calculated G in the case of the most efficient cell (i.e., very rough TCO substrate and ITO/Ag contact). G reaches the maximum value of 6 for 800 nm. This value is much lower than the light-trapping limit ($G=50$) previously presented. This important difference comes from residual absorptances occuring in the electrodes and in the p and n layers. For the less efficient structure, G saturates at 3. Our calculated maximum values of G for these solar cells are in good agreement with values proposed by Shade and Smith[3] ($G=3$) and also by Walker, Hollingsworth, and Madan[18] ($G=3$–5).

VIII. CONCLUSION

We have reported a new semiempirical approach to model the optical properties of a-Si:H p-i-n solar cells. In order to describe the optical properties induced by the TCO roughness, we assume that the thin-film stacks have two rough interfaces: the TCO/p and the n/metal interfaces. The specular light propagation is analyzed by the usual matrix method, where the amplitude reflection and refraction specular coefficients are assumed to be proportional to the Fresnel coefficients. The light coherence and the angular dependence of the specular coefficients are taken into account. The diffuse reflectance and transmittance for the front and back rough interfaces, considered as input parameters, are either experimentally measured at four visible wavelengths or adjusted in order to fit the experimental characteristics. A second matrix algorithm procedure allows the calculation of the absorptances due to light scattering in reasonable computation time. The diffuse reflectance and transmittance are comparable to values found in the literature, but the modeling demonstrates better results than the usual analytical but more restrictive approaches. Improvement mainly comes from the specular light propagation treatment. The numerical simulation allows the estimation of the power balance in realistic solar-cell structures. Optical losses in the electrodes, in the doped layers and due to reflection, can be accurately calculated. The absorptance enhancement factor due to light trapping reaches the value $G=6$ for the most efficient structure studied.

ACKNOWLEDGMENTS

We gratefully thank H. J. Drouhin and C. Hermann from the Laboratoire de Physique de la Matière Condensée of the Ecole Polytechnique, for lending us the Krypton laser, R. Morano from the Laboratoire de Physique Nucléaire des Hautes Energies of Ecole Polytechnique, for assistance in the computations, and E. Cornil from SOLEMS S.A., for providing samples. We thank S. Vallon from the Laboratoire de Physique des Interfaces et des Couches Minces for helpful discussions.

[1] T. Yoshida, S. Jujikake, H. Fujisawa, S. Saito, T. Sasaki, Y. Ichikawa, and H. Sakai, in *Proceedings of the 10th European Photovoltaic Solar Energy Conference*, Lisbon, Portugal, April, 1991, edited by A. Luque, G. Sala, W. Palz, G. Dos Santos, and P. Helm (Kluwer Academic, Dordrecht, 1991), p. 1193.
[2] H. W. Deckman, C. R. Wronski, H. Witzke, and E. Yablonovitch, Appl. Phys. Lett. **42**, 968 (1983).
[3] H. Shade and Z. Smith, J. Appl. Phys. **57**, 568 (1985).
[4] J. Morris, R. R. Arya, J. G. O'Dowd, and S. Wiedeman, J. Appl. Phys. **67**, 1079 (1990).
[5] E. Yablonovitch, J. Opt. Soc. Am. **72**, 899 (1982).
[6] E. Yablonovitch and G. D. Cody, IEEE Trans. Electron. Devices **ED-29**, 300 (1982).
[7] H. A. Macleod, *Thin Film Optical Filters* (Hilger, Bristol, 1986).
[8] F. Abeles, Ann. Phys. Paris **5**, 596 (1950); **5**, 706 (1950).
[9] P. Bousquet, F. Flory, and P. Roche, J. Opt. Soc. Am. **71**, 1115 (1981).
[10] D. Maystre, J. Optics (Paris) **15**, 43 (1984).
[11] M. Saillard and D. Maystre, J. Opt. Soc. Am. A **7**, 982 (1990).

[12] J. A. DeSanto, in *Multiple Scattering and Waves in Random Media*, edited by P. L. Chow, W. E. Kobler, and G. C. Papanicolaou (North-Holland, Amsterdam, 1981), p. 123.
[13] J. G. O'Dowd, Sol. Energy Mater. **16**, 383 (1987).
[14] H. Shade and Z. Smith, Appl. Opt. **24**, 3221 (1985).
[15] F. Leblanc, J. Perrin, J. M. Siéfert, J. Schmitt, and C. Godet, in Technical Digest of the 5th International Photovoltaic Science and Engineering Conference (PVSEC-5), Kyoto, Japan, Nov. 1990, p. 253.
[16] R. G. Gordon, J. Proscia, F. B. Ellis, and A. E. Delahoy, Sol. Energy Mater. **18**, 263 (1989).
[17] C. Walker, R. E. Hollingsworth, J. del Cueto, and A. Madan, Mater. Res. Soc. Symp. Proc. **70**, 563 (1986).
[18] C. Walker, R. E. Hollingsworth, and A. Madan, Mater. Res. Soc. Symp. Proc. **95**, 527 (1987).